1   **Assessing global-scale organic matter reactivity patterns in marine**

2   **sediments using a lognormal reactive continuum model**

3   **Sinan Xu[1,2,3], Bo Liu[3], Sandra Arndt[4], Sabine Kasten[3,5], and Zijun Wu[1*]**

4   [1]State Key Laboratory of Marine Geology, School of Ocean and Earth Science, Tongji

5   University, Shanghai, 200092, China

6   [2]The Key Laboratory of Gas Hydrate, Ministry of Natural Resources, Qingdao Institute of

7   Marine Geology, Qingdao, 266071, China

8   [3]Alfred Wegener Institute Helmholtz Centre for Polar and Marine Research, 27570

9   Bremerhaven, Germany

10   [4]Department of Geosciences, Environment and Society, Universit´e Libre de Bruxelles,

11   Avenue Franklin Roosevelt 50, 1050 Brussels, Belgium

12   [5]Faculty of Geosciences, University of Bremen, 28359 Bremen, Germany

13

14   **Correspondence to: Zijun Wu (wuzj@tongji.edu.cn)**

15

16   **Abstract**

17   Organic matter (OM) degradation in marine sediments is largely controlled by its

18   reactivity and profoundly affects the global carbon cycle. Yet, there is currently no general

19   framework that can constrain OM reactivity on a global scale. In this study, we propose a

20   reactive continuum model based on a lognormal distribution (l-RCM), where OM

21   reactivity is fully described by parameters μ (the mean reactivity of the initial OM bulk

22   mixture) and σ (the variance of OM components around the mean reactivity). We use the

23   l-RCM to inversely determine μ and σ at 123 sites across the global ocean. The results show

that the apparent OM reactivity ($<k>=\mu \cdot \exp(\sigma^2/2)$)) decreases with decreasing

sedimentation rate (ω) and show that OM reactivity is more than three orders of magnitude

higher in shelf than that in abyssal regions. Despite the general global trends, higher than

expected OM reactivity is observed in certain ocean regions characterized by great water

depth and/or pronounced oxygen minimum zones, such as the Eastern-Western Coastal

Equatorial Pacific and the Arabian Sea, emphasizing the complex control of the

depositional environment (e.g., OM flux, oxygen content in the water column) on benthic

OM reactivity. Notably, the *l*-RCM can also highlight the variability of OM reactivity in

these regions. Based on inverse modeling results in our dataset, we establish the significant

statistical relationships between $<k>$ and ω, and further map the global OM reactivity

distribution. The novelty of this study lies in its unifying view, but also in contributing a

new framework that allows predicting OM reactivity in data-poor areas based on readily

available (or more easily obtainable) information. Such a framework is currently lacking

and limits our abilities to constrain OM reactivity in global biogeochemical and/or Earth

System Models.

1 Introduction

Marine sediments act as the ultimate sink for organic carbon. The size and reactivity of

the benthic organic matter (OM) reservoir is a critical component of the global carbon cycle

(Arndt et al., 2013). In particular, the reactivity of benthic OM imposes a substantial control

on the magnitude of benthic carbon export and burial over geological timescales due to the

recycling of organic carbon by dissimilatory microbial activity in the deep biosphere

(Boudreau, 1992; Zonneveld et al., 2010), the dissolution and precipitation of carbonates

47 (Meister et al., 2022; Nöthen and Kasten, 2011), and the production of methane (Dickens

48 et al., 2004; Whiticar, 1999). Decades of research have shown that OM reactivity is

49 controlled by both the nature of the OM (origin, composition and degradation state), as

50 well as its environmental and depositional conditions (e.g., redox conditions, sedimentation

51 rate, mineral protection, microbial community composition and biological mixing)

52 (Burdige, 2007; Egger et al., 2018; Hartnett et al., 1998; Hedges and Keil, 1995; Larowe

53 et al., 2020a; Zonneveld et al., 2010). However, due to the complex and dynamic nature of

54 the main controls on OM reactivity, the specific relative significance of these controlling

55 factors remains poorly quantified. Consequently, OM degradation models generally do not

56 explicitly describe the influence of environmental and depositional factors on OM

57 reactivity and its evolution but rather apply simplified parametrizations (Freitas et al., 2021;

58 Pika et al., 2021). Over the past decades, several models have been developed and

59 successfully used to quantify OM degradation in marine sediments. They can be broadly

60 divided into two groups: discrete models, such as the (multi) *G* model (Berner, 1964;

61 Jørgensen, 1978), and continuum models, such as the reactive continuum model (RCM)

62 (Boudreau and Ruddick, 1991) and the power model (Middelburg, 1989).

63 Discrete models divide the bulk OM pool into several discrete fractions, each with its

64 own constant reactivity (Fig.1A). The 1-*G* model is the earliest OM degradation model,

65 which is based on the assumption that OM degrades according to first order dynamics with

66 a single constant degradation rate constant (Berner, 1964). The multi-*G* model, on the other

67 hand, divides OM into several fractions, and each fraction is degraded according to a first-

68 order rate with a fraction-specific reactivity (Jørgensen, 1978). Although multi-*G* models

69 successfully fit observed OM degradation dynamics when comprehensive data sets are

70   available, their application on a global scale is complicated by the need to partition the OM

71   reactivity into a finite number of fractions and define their reactivities. A multi-G model

72   with n discrete OM fractions requires constraining $2n$-1 parameters and is, thus, over-

73   parametrized (Jørgensen, 1978). Nevertheless, because of its mathematical simplicity and

74   wide use, multi-G models have been used in a range of diagenetic models designed for the

75   global/regional scale (e.g., CANDI, MEDIA, MEDUSA, and OMEN SED) (Boudreau,

76   1996; Meysman et al., 2003; Munhoven, 2007; Pika et al., 2021). Constraining the $2n$-1

77   OM degradation model parameters for these global-scale applications is not

78   straightforward. Early strategies for constraining the reactivity of OM on a global scale

79   have focused on deriving empirical relationships between OM reactivity and single, easily

80   observable characteristics of the depositional environment (water depth, sedimentation rate,

81   or OM flux) (Arndt et al., 2013). However, poor statistically significant link between OM

82   reactivity and depositional environment could be established ($R^2<0.1$) after compiling

83   published multi-G model's parameters across a wide range of depositional environments,

84   model complexities as well sediment depths/ burial time scales (Arndt et al., 2013).

85   Reactive continuum models (RCMs) are an alternative to discrete models. They assume

86   that OM compounds are continuously distributed over a wide range of reactivities. The

87   degradation rate can be described as the sum of an infinite number of discrete fractions,

88   each degraded according to first-order kinetics (Boudreau and Ruddick, 1991), as

89    $$G(t) = \int_0^\infty G(0) \cdot g(k,0) \cdot e^{-kt} dk \qquad (1)$$

90   where $G(t)$ is OM content at time t, $G(0)$ is OM content at the sediment-water interface

91   (SWI), k is the first-order degradation rate constant, and $g(k,0)$ is the initial reactivity

92   distribution of OM at the SWI. The key to constructing an RCM is to select a continuum

distribution that describes the OM reactivity at the SWI (Fig. 1B). Considering the k value in Eq. 1 must be greater than zero ($k > 0$), some of the all-axial statistical distributions ($x \in$ (-∞, +∞)) are not appropriate for constructing RCM (e.g., Normal distribution, Fig.1D$_1$). Boudreau and Ruddick. (1991), following Aris (1968) and Ho et al. (1987), proposed to use a Gamma distribution (γ-RCM, Fig.1D$_2$) due to its mathematical properties and its ability to capture the observed dynamics:

$$g(k, 0) = \frac{a^v \cdot k^{v-1} \cdot e^{-ak}}{\Gamma(v)} \tag{2}$$

where a is the average age of the OM at the SWI, v is the shape parameter, and $\Gamma(v)$ is the Gamma function. In addition, Middelburg. (1989) empirically derived a power law from a large data compilation of measured OM reactivity (Fig.1C), which is mathematically equivalent to the γ-RCM. The advantage of the continuum models over the discrete models is that they merely require constraining two free parameters to capture the widely observed continuous decrease in OM reactivity with degradation time/depth. Recently, γ-RCM has been used to inversely determine the free γ-RCM parameters, and thus benthic OM reactivity, from observed POC and sulfate depth profiles across a wide range of different depositional environments (Freitas et al., 2021). Although results revealed broad global patterns, no significant statistical relationship ($R^2 < 0.46$) between the parameters (a and v) of the γ-RCM (Arndt et al., 2013) and characteristics of the depositional environment could be found, and constraining OM degradation model parameters on the global scale thus remains difficult.

Here, we present an RCM based on a lognormal distribution (Forney and Rothman, 2012b):

$$g(k, 0) = \frac{1}{k \cdot \sigma \cdot \sqrt{2\pi}} \cdot e^{-(\ln k - \ln \mu)^2 / (2\sigma^2)} \tag{3}$$

116 where $\ln \mu$ is the mean of $\ln k$, and σ^2 is the variance of $\ln k$ (Fig.1D$_3$). Parameter μ

117 determines the mean reactivity of the initial OM bulk mixture and parameter σ reflects the

118 spread of OM components around the mean reactivity.

119   The lognormal distribution is formed by the multiplicative effects of random variables,

120 which is commonly observed in nature (e.g., the radioactivity of elements in the crust, the

121 incubation period of infectious diseases, and ecological species abundance) (Limpert et al.,

122 2001). In the ocean system, the rates of ocean primary production and biological carbon

123 export also fit the lognormal distribution (Cael et al., 2018). The degradation of OM in

124 natural ecosystems is controlled by a network of biologically, physically, and chemically

125 driven processes (Forney and Rothman, 2014), so the variables raised from such

126 multiplicative processes are often followed by a lognormal distribution. Forney and

127 Rothman (2012b) showed that litter bag OM incubation data is indeed best described by a

128 lognormal distribution of rates.

129
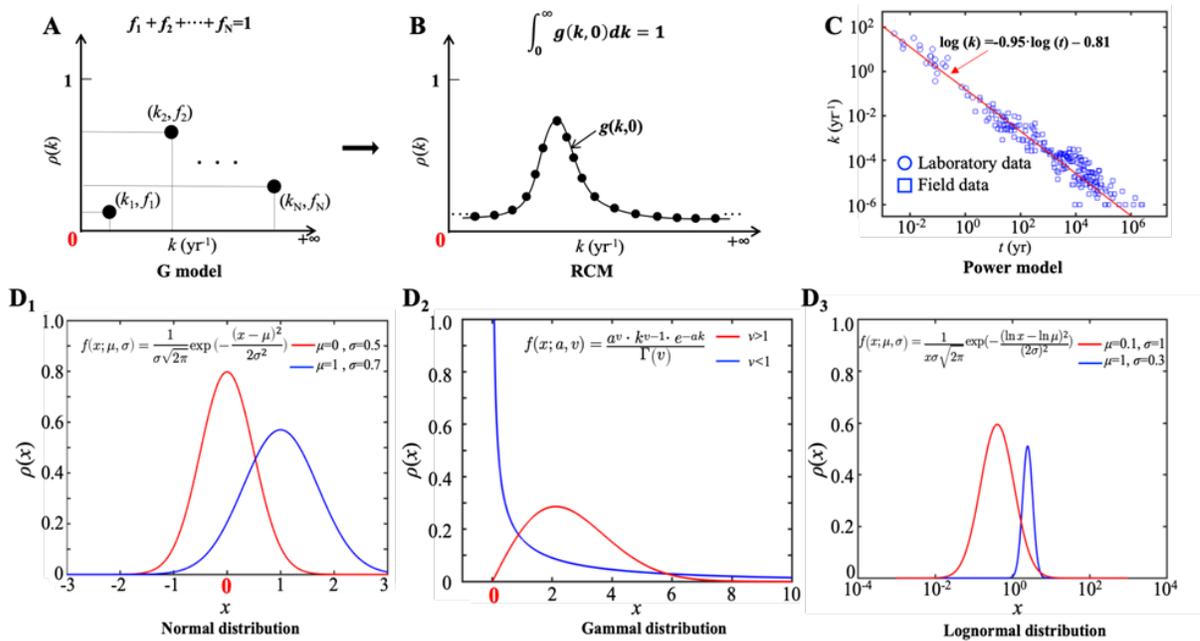
Figure 1. Schematic diagram of different OM degradation models. A: G model, B: RCM, C: Power model and D: Common continuum distribution functions. The x coordinate denotes the variation range of values, and the y coordinate denotes the probability density distribution (ρ) (D_1: the Normal distribution, a typical all-axis distribution, D_2: the Gamma distribution, a typical semi-axis ($x>0$) distribution, and D_3: the Lognormal distribution, a typical semi-axis ($x>0$) distribution).

In this study, we first compared the l-RCM with other OM degradation models and analyzed the advantages of the l-RCM in describing the OM reactivity distribution. Then we simulated OM degradation in marine sediment at 123 global sites using the l-RCM. Based on inverse modeling results in our dataset, we established the empirical formulas of OM reactivity vs sedimentation rate and further mapped the global OM reactivity distribution. This study provides a new framework for assessing OM reactivity on regional/global scales and predicting OM reactivity in data-poor areas based on easily obtainable environmental parameters (e.g., sedimentation).

2 Materials and methods

2.1 OM degradation model approach

We constructed an RCM with lognormal distribution (l-RCM) to simulate the OM degradation in marine sediments. The $g(k,0)$ we used in Eq. 1 is the lognormal distribution (Eq.3). Because of the tail of $g(k,0)$, the mean rate constant for bulk OM degradation or the apparent degradation rate of the bulk OM ($<k>$) is greater than the median μ, as follows:

$$< k >= \int_0^\infty k \cdot g(k,0)dk = \mu \cdot e^{\sigma^2/2} \tag{4}$$

2.2 Inverse model approach

154   Here, we used 123 published datasets of OM depth profiles across a wide range of

155   different depositional environments that have been sourced from published literature

156   (Middelburg, 1989; Arndt et al., 2013; Middelburg et al., 1997) and the IODP database

157   (Fig.2, Supplementary Table S1) to inversely determine the μ and σ parameters. We also

158   analyzed a small number (n=12) of laboratory experiment data on OM degradation

159   (Middelburg, 1989), as well as OM degradation data (n=16) from terrestrial soils (Katsev

160   and Crowe, 2015). We followed the inverse modeling approach by Forney et al.(2012a) to

161   identify the best-fitting parameters μ and σ based on the Newton method.
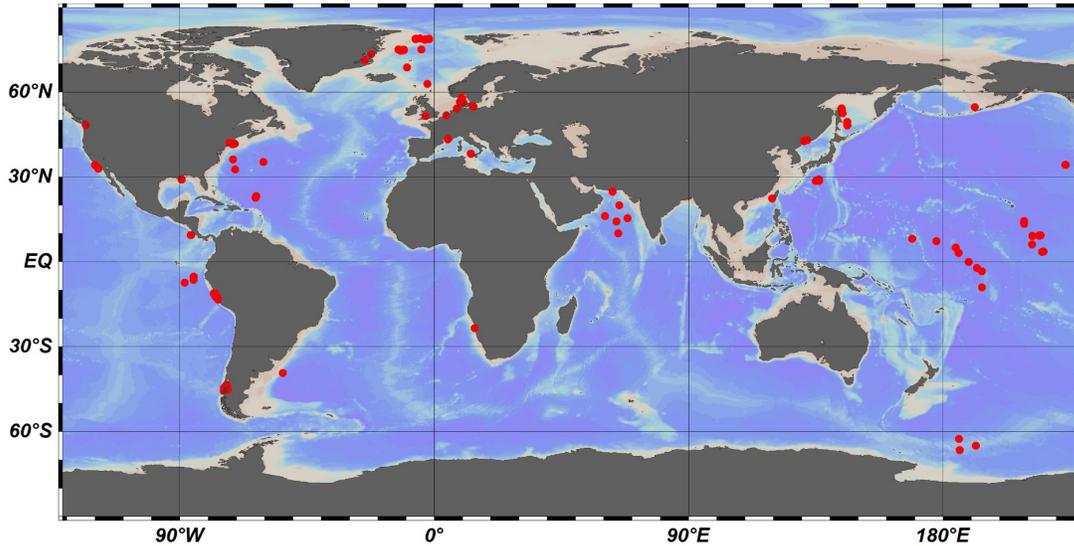
162
163   **Figure 2. Global distribution of investigated sites.**

164

165   Notably, the burial time was correlated with the porosity. A simple exponential function

166   was used to describe porosity in sediments:

$$\varphi(x) = \varphi_0 \cdot e^{-\lambda x} \qquad (5)$$

168   where φ_0 is the values of porosity at the SWI, λ is the attenuation coefficient, and x is

169   depth. Considering the compaction impacts on OM degradation, the burial time

170   corresponding to each depth in the OM profile can be calculated as:

$$171 \qquad t(x) = \int_0^x \omega^{-1} dx = \frac{x}{\omega_f} + \frac{(\varphi_0 - \varphi_f)}{(1-\varphi_f)\cdot\lambda\cdot\omega_f} \cdot (e^{-\lambda\cdot x} - 1) \qquad (6)$$

172   where φ_f is the values of porosity at larger depths, calculated from Eq. 5 and the pre-set

173   simulation depth. If the porosity data were not available, the global set as: shelf regions (φ_0:

174   0.45, λ: 0.5×10^{-3}), slope regions (φ_0: 0.74, λ: 1.7×10^{-4}), and abyssal regions (φ_0: 0.7, λ:

175   0.85×10^{-3}) (LaRowe et al., 2020b).

176   **2.3 Global upscaling of sedimentation rate**

177   The inversely determined μ, σ couples of all investigated sites were then used in a linear

178   regression method to derive the empirical relationships between OM parameters μ, σ, $<k>$

179   and the local sedimentation rates (ω). A correction factor was applied to account for the

180   skewness bias inherent in the back conversion from a log-log transformed linear regression

181   model to arithmetic units. The newly derived empirical relationships between $<k>$ and ω

182   were then used to calculate global maps of OM reactivity at the SWI on a $1°\times1°$ grid cell

183   of the world ocean. At each grid point, ω was estimated based on the empirical relationship

184   between ω (ω in cm yr^{-1}) and the water depth (z in m) (Eq.7, Fig.3), derived from 260

185   observations on the global continental shelves (Burwicz et al., 2011), complemented here

186   by an extra 360 sites including abyss regions (data from Arndt et al. (2013), Egger et al.

187   (2018)).

$$188 \qquad \omega(z) = \frac{0.4}{1+\left(\frac{z}{200}\right)^{3.5}} + \frac{0.004}{1+\left(\frac{z}{4500}\right)^{17}} \qquad (7)$$
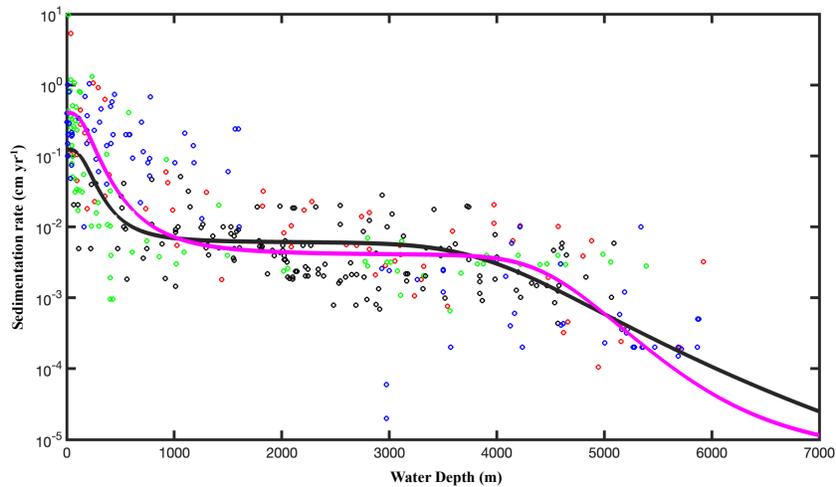
Figure 3. Relationship between Sedimentation rate (w) and water depth (z in m). The data are taken from Arndt et al. (2013) (black circles), Egger et al.(2018) (pink circles), Betts and Holland (1991) (red circles), Colman and Holland (2000) (green circles), and Seiter et al. (2004) (blue circles). The pink line is the fitting result according to Eq. 7 (R^2=0.57), and the black line is the fit obtained from the data of Burwicz et al. (2001) (R^2=0.43).

Considering the geographic differences in depositional environments and to describe the global distribution of sedimentary OM reactivity in more detail, we divided the global ocean into 30 different regions (Table 2, Fig.4) using 5600 single measured data of OM content in global surface sediment (<5 cm sediment depth) and the previously used combined qualitative and quantitative geostatistical methods (Seiter et al., 2004).
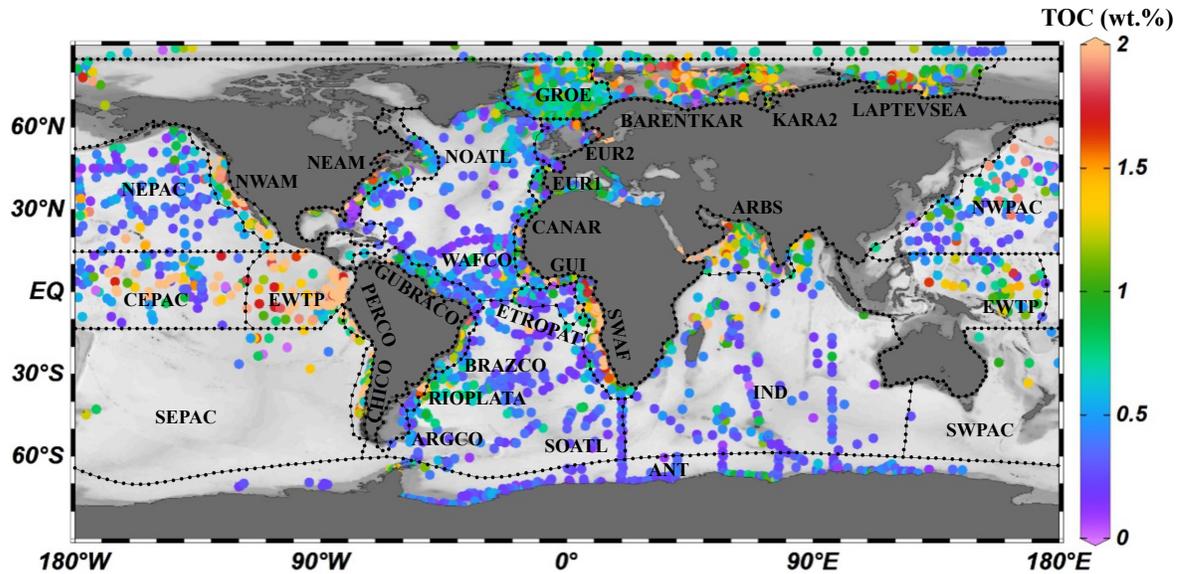
Figure 4. The 30 different regions of the global ocean were divided using 5600 single measured data of OM content (wt.%) of surface sediments

3 Results and discussion

3.1 OM reactivity distribution described by the *γ*-RCM and the *l*-RCM

To compare OM reactivity distribution described by the *l*-RCM and the *γ*-RCM, we determined the best fit to the eight OM datasets reported by Boudreau and Ruddick. (1991). The results show that both RCMs fit the data equally well, as illustrated by the high coefficient of determination for each fit ($R^2 > 0.9$, Table 1 and Fig.5). However, the *l*-RCM and the *γ*-RCM differ in their ability to find a unique solution and in their respective probability density functions of OM reactivity ($\rho(k)$). For example, Fig.6A and 6B show the best-fit OM profiles for two contrasting sites: BX-6 on the shelf and DSDP 58 in the abyssal region. The inversely determined parameters at the two sites are $\mu = 2.23 \times 10^{-3}$ yr^{-1}, $\sigma = 2.03$ at BX-6, and $\mu = 6.11 \times 10^{-5}$ yr^{-1}, $\sigma = 1.66$ at DSDP 58 by the *l*-RCM. At BX-6, the

best-fitting parameters by the γ-RCM are $v = 0.278$ and $a = 22.5$, and at DSDP 58, $v = 1.08$ and $a = 20224$. According to the parameter sensitivity analysis, the R^2 of the fitted results remains greater than 0.9 when a and v change substantially simultaneously (Fig.6D, Supplementary Table S2, Fig.S1, S2, and S3). As a result, different combinations of a and v can fit the data equally well. For example, simultaneously increasing v and a ($v = 0.5$ and $a = 53$) at site BX-6 or decreasing v and a ($v = 0.5$ and $a = 4024$) at site DSDP 58 lead to a slight change in R^2. Adding additional measured data, such as depth profiles of porewater sulfate and methane concentrations, can help find a unique solution (Freitas et al., 2021). In contrast, the best-fit parameters μ and σ are unique in the l-RCM, and even small changes in either parameter can lead to abysmal fitting results (Fig.6D). The second difference between the two models concerns the shape of the probability distribution $\rho(k)$. Statistically, the features of the Gamma distribution vary with the value of v. If $v < 1$, $\rho(k)$ tends to positive infinity when k approaches zero. In contrast, if $v > 1$, $\rho(k)$ tends to zero when k approaches zero. Hence, the characteristics of the Gamma distribution under different v values are difficult to visually compare the OM reactivity distributions at site BX-6 ($v < 1$) and DSDP 58 ($v > 1$) (Fig.6C). Compared with γ-RCM, the l-RCM can better distinguish OM reactivity distribution at different sites.

Table 1. List of model parameters and coefficients of determination (R^2) for the fitting result of γ-RCM and l-RCM.

Core	γ-RCM			l-RCM		
	v (-)	a (yr)	R^2	μ (yr^{-1})	σ (-)	R^2
Foam	0.152	4.2	0.930	2.2×10^{-3}	3.725	0.923
SCR-44	0.202	70.4	0.929	4.4×10^{-4}	2.706	0.922
BX-6	0.278	22.5	0.929	2.24×10^{-3}	2.031	0.936
PC2&TW2	0.052	0.16	0.937	5.5×10^{-5}	6.688	0.947
10141&2	0.193	10184	0.935	1.9×10^{-6}	3.289	0.936
7706-41K	0.910	141.3	0.974	9.5×10^{-3}	0.899	0.972

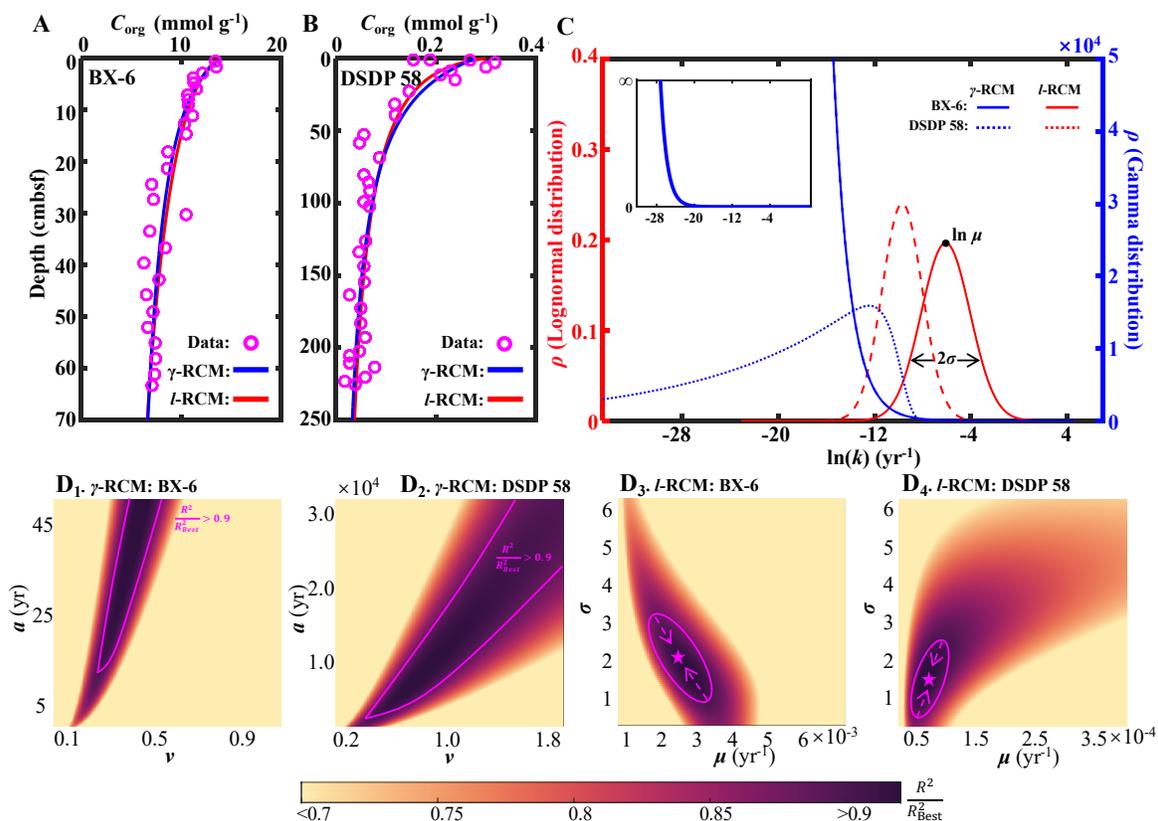|						
7706-36	0.804	231.7	0.978	4.79×10^{-4}	1.089	0.980
DSDP58	1.080	20224	0.917	6.11×10^{-5}	1.663	0.921

237
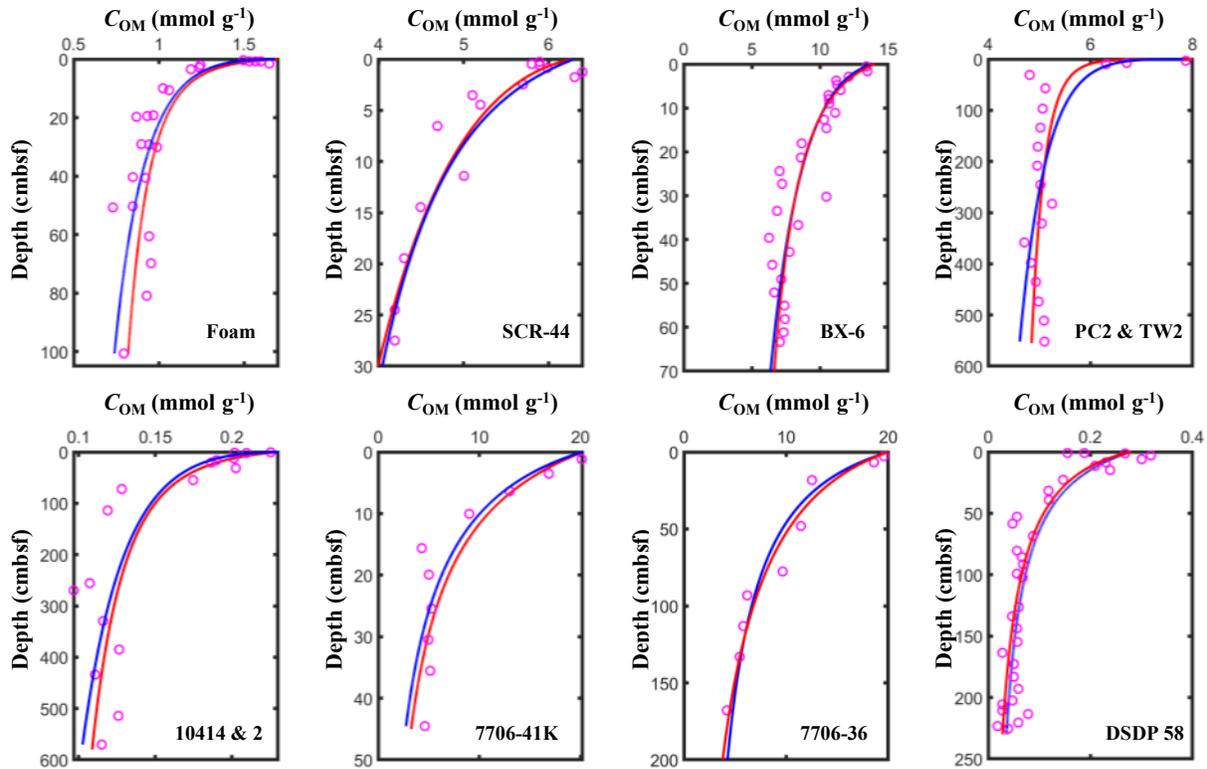
238
239 **Figure 5. Fitting results of the *l*-RCM and the *γ*-RCM.** The pink dots are the measured

240 OM data, the red lines are *l*-RCM fitting results, and the blue lines are *γ*-RCM fitting results.

241

Figure 6. Comparison of *l*-RCM and *γ*-RCM. A, **B**: the fitting results of the *l*-RCM and the *γ*-RCM for site BX-6 and DSDP 58. **C**: OM reactivity distribution from *l*-RCM and *γ*-RCM. Top inset, Gamma distribution at site BX-6 at a larger y-axis. **D**: Distribution of R^2/R^2_{Best} for parameter sensitivity analysis of the *γ*-RCM and the *l*-RCM at sites BX-6 and DSDP 58. The pink lines in the D_1 and D_2 denote the range that $R^2/R^2_{\text{Best}}>0.9$ in the *γ*-RCM. The R^2/R^2_{Best} in the *l*-RCM converges as the pink arrows in the D_3 and D_4, ultimately reaching the best fitting results as the pink pentagrams.

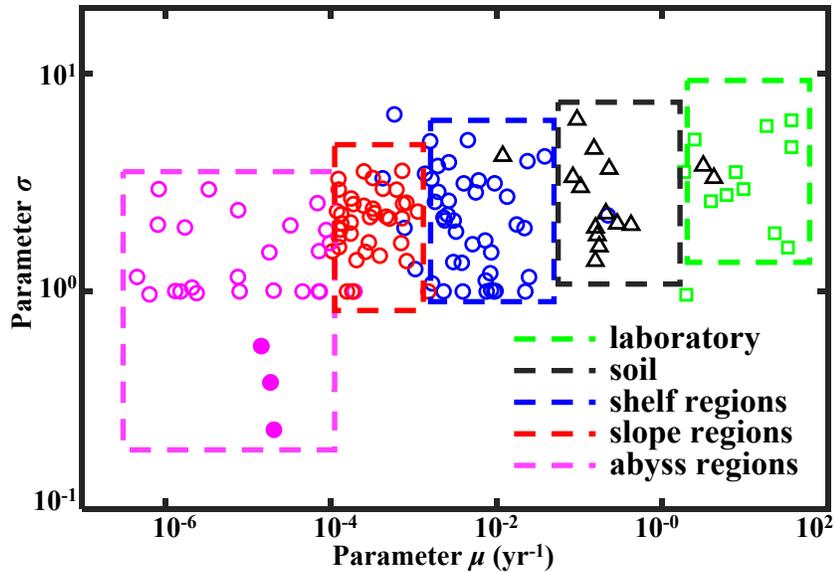## 3.2 Regional distribution of OM reactivity

In the *l*-RCM, parameter μ represents the mean reactivity of the OM fractions, which dominates the rate of OM degradation (Supplementary Fig.S2), and parameter σ describes the homogeneity of OM fractions, with larger σ value indicating more heterogeneous mixture of OM (Forney et al., 2012b). The inverse determination of the *l*-RCM parameters

256   μ and σ across the wide range of different depositional environments allows quantitative

257   insights into OM reactivity and provides essential information on the main environmental

258   controls on OM reactivity. Fig.7 illustrates the inversely determined μ-σ for all 123 depth

259   profiles of marine sediment POC investigated in this study and compares them with

260   inversely determined parameters from published soil and laboratory incubation data. It

261   highlights the large inter- and intraregional variability of best-fit μ (10^{-6}–10^2 yr^{-1}) and σ

262   (0.2–6). However, despite the large variability, it also reveals broad global patterns in μ

263   and σ. Notably, best-fit μ-σ couples form environmental clusters along a μ gradient, with

264   the highest μ being determined for laboratory degradation experiments of fresh

265   phytoplankton (Garber, 1984; Westrich and Berner, 1984) (μ=10^0–10^2 yr^{-1}), followed by

266   soil incubation under natural (Katsev and Crowe, 2015), yet still idealized conditions

267   (μ=10^0–10^1 yr^{-1}), while OM degraded in marine sediments generally reveals lower

268   inversely determined μ<10^0 yr^{-1}. The higher μ values determined for soil OM seemingly

269   contradict the widely accepted notion that soil OM is generally less reactive than marine

270   OM (Larowe et al., 2020a; Zonneveld et al., 2010). However, this apparent contradiction

271   can be explained by the idealized conditions of the incubation experiments (e.g., only one

272   type of material, some of which had nitrogen added), as well as the degradation state of the

273   investigated OM. Although soil OM is structurally less reactive (Hedges and Keil, 1995;

274   Zonneveld et al., 2010), the soil incubation experiments were conducted with initially

275   undegraded material. In contrast, OM deposited in marine sediments consists of a complex

276   mixture of OM from autochthonous and allochthonous sources that is altered to various

277   degrees during transit from its source to the sediment (Hewson et al., 2012).

278   In addition to the difference between incubation data and field observations, Fig.7 also

279   reveals a three order of magnitude decrease in inversely determined μ for OM from the

280   shelf (10^{-3}–10^{-1} yr^{-1}) to the slope (10^{-4}–10^{-3} yr^{-1}), and ultimately abyssal regions (<10^{-4} yr^{-}

281   ^{1}). In addition, shelf and slope regions also generally reveal a larger σ (1–3), while abyssal

282   regions display a narrower σ range (0.5–1). This observed progressive decrease in μ and σ

283   from the shelf to the abyssal ocean confirms previously observed patterns (Arndt et al.,

284   2013; Freitas et al., 2021; Zonneveld et al., 2010) and reflects the interaction between OM

285   structure (or its source) and the degree of alteration/pre-processing as OM transits from its

286   original source to the ultimate sedimentary sink. In the dynamic shelf regions, highly

287   variable OM loads from different sources, including *in*-situ produced marine OM, laterally

288   transported, pre-processed terrestrial or marine OM, are often physically protected from

289   further erosion/deposition cycles due to high suspended sediment loads (Arndt et al., 2013;

290   Larowe et al., 2020a). As a result, benthic OM is composed of a complex mixture of fresh

291   and pre-aged compounds of highly variable (hence larger σ of the initial distribution*)*, yet

292   generally higher reactivity. On the upper and mid-continental slopes, intensive lateral

293   and/or vertical transport processes or the abrupt relocation of sediment result in similar

294   complex mixtures of OM (hence similar σ of the initial distribution) (Larowe et al., 2020a).

295   However, transport timescales are often longer due to the greater water depths and distance

296   to land. The deposited OM is generally more degraded and thus less reactive than in shelf

297   environments. In contrast, benthic OM in abyssal regions is mainly derived from marine

298   production (Rowe and Staresinic, 1979; Larowe et al., 2020a). During its slow settling

299   through the water column, highly reactive OM compounds are rapidly degraded, and only

300   the less reactive compounds persist and settle onto the sediment (Dunne et al., 2007). The

301 values of μ and σ in the abyssal regions are thus significantly smaller than in the shelf and

302 slope regions. The decrease of μ and σ from the shelf to abyssal regions reveals a decline

303 in reactivity during lateral transport of OM, where μ mainly controls the overall reactivity

304 and σ indicates the coverage of the main component of OM.

305

Figure 7. Regional distribution of OM reactivity. Distribution of parameters σ and μ in
different regions. Pink solid circles denote fitting results of sites in the NEPAC with
extremely low OM reactivity.

309

3.3 Global distribution patterns of OM reactivity

311 Parameters μ and σ together control the degradation process of OM, which can be further

312 described by the apparent degradation rate of the bulk OM ($<k>$). Sedimentation rate (ω)

313 is a widely observed and comparably easy to measure proxy for local depositional

314 conditions with sizable global data sets or empirical formulas available (Burwicz et al.,

315 2011). Fig. 8A, 8B and 8C show the global decreasing trend of μ, σ and $<k>$ with ω for the

316 general sea regions (shelf (<200m), slope (200–2000m), and abyss (>2000m)).The active

OM fractions (e.g., sugars and proteins) are preferentially exhausted during the lateral transport of OM from the shelf to the abyssal regions, leading to a decrease in the mean OM reactivity (μ, Fig. 8A), and thus OM is mainly composed of refractory components (σ, Fig. 8B). Due to the multiple sources of OM in the shelf regions, including fresh and older OM imported laterally by inland rivers, and OM settled from the euphotic layer (LaRowe et al., 2020a), the values of the values of μ, σ and $<k>$ fluctuates significantly. However, the general trend is superimposed by a large variability and apparent reactivity $<k>$ in specific environments, notably deviating from this generally observed trend. More specifically, higher μ and σ values and, thus, higher OM reactivities occur in the Eastern-Western Coastal Equatorial Pacific (EWEP), Southwestern-Africa continental margin (SWAF), Northwestern-America continental margin (NWAM), and the Arabian Sea (ARBS) regions. These results are completely consistent with prior observations and model results (Arndt et al., 2013) and can be directly linked to the prevailing water-column redox and depositional conditions. High benthic OM reactivities have previously been reported for depositional environments that are characterized by a dominance of marine algal OM (Hammond et al., 1996) and strong lateral transport processes (e.g., SWAF, NWAM) (Arndt et al., 2013). Consequently, the larger values of all μ and σ, and $<k>$ occur in the inverse modelling results for these depositional environments (Fig. 8). Furthermore, the reactivity of sedimentary OM is considerably influenced by oxygen content or more precisely, by oxygen exposure time in the water column and at the seafloor (Aller, 1994; Hartnett et al., 1998; Hedges and Keil, 1995; Mollenhauer et al., 2003; Zonneveld et al., 2010). Lower oxygen concentrations, as present in these regions in the form of pronounced oxygen minimum zones (OMZs), will slow down the degradation of OM both in the water

column and at the sediment surface (Jørgensen et al., 2022). This enables the burial of more reactive OM into the sediments and thus results in the occurrence of high sedimentary OM reactivity in these regions despite great water depth (e.g., ARBS, EWTP) (Arndt et al., 2013; Bogus et al., 2012; Ingole et al., 2010; Luff et al., 2000; Volz et al., 2018). The *l*-RCM not only captures the broad patterns of OM reactivity across the global seafloor even better than previous models, but also provides statistically more significant relationships between OM reactivity ($<k>$) and sedimentation rate (ω) than inversely determined parameters of γ-RCM ($R^2<0.46$) and discrete models ($R^2<0.1$) (Arndt et al., 2013). Considering that no robust quantitative framework exists at this stage to predict OM reactivity as a function of easily observable environmental parameters, the *l*-RCM provides an excellent first-order predictor and a step forward in assessing the global distribution patterns of OM reactivity, despite the poor relationship between $<k>$ and ω for these special regions (e.g., EWEP, SWAF, NWAM, and ARBS).
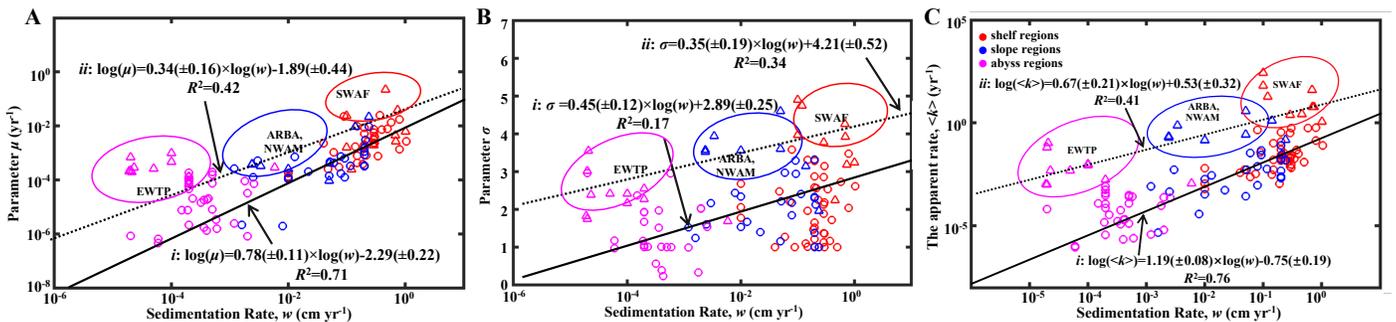
Figure 8. Global distribution patterns of OM reactivity. A. Log-log plot of ω and μ. B. Log-log plot of ω and σ. C. Log-log plot of ω and $<k>$. The solid black line (*i*) denotes linear regression for shelf, slope, and abyssal regions. The black dotted line (*ii*) denotes linear regression for high OM reactivity regions, including the EWTP, ARBS, NWAM, and SWAF regions.

360   Based on the empirical relationships in Fig.8 (i for the general water depth-related

361   regions, ii for the specific regions (EWTP, ARBS, NWAM, and SWAF)), and the water

362   depth–ω relationship (Eq.5), we finally derived, to our knowledge, the world's first map

363   of the global distribution of parameter μ, σ, and $<k>$ (Fig.9). Using the relationship between

364   water depth, ω, and $<k>$ (Fig.3 and Fig.8C), we further estimated the mean apparent OM

365   reactivity ($<K_{region}>$) in the 30 regions of global ocean (Table 2). Furthermore, the

366   heterogeneity of the OM reactivity distribution in global marine sediments is well

367   illustrated in Fig. 9. Specifically, higher μ (Fig.9A), σ (Fig.9B), and OM reactivity (Fig.9C)

368   is reflected in shelf regions, particularly in northern Atlantic provinces with high latitudes

369   (e.g., Barents Sea ($<K_{region}> \approx 0.02$ yr^{-1}), Laptev Sea ($<K_{region}> \approx 0.03$ yr^{-1}), and Kara Sea

370   ($<K_{region}> \approx 0.01$ yr^{-1})), due to shallower water depths and high OM fluxes from inland

371   (Burwicz et al., 2011; Seiter et al., 2004). Besides that, the global map also highlights the

372   extremely low OM reactivity, especially in some regions, as indicated by the absence of

373   sulfate-methane transition (SMT) (e.g., the NE-Pacific, NEPAC) (Eggert et al., 2018) and

374   central ocean gyre regions (e.g., South Pacific Gyre) (LaRowe et al., 2020b). Deeper water

375   depth (>5000m), relatively low OM content (~0.2wt.%), and the old OM age (>10^4 years)

376   result in comparably lower μ and σ values (Fig.9A and 9B) and, thus, extremely low benthic

377   OM reactivity ($<K_{region}> \approx 10^{-4}$ yr^{-1}) (Kallmeyer et al., 2012, Müller and Suess, 1979).

378   Normally, greater water depth enhances oxygen exposure time for OM degradation, and

379   thereby reduce the reactivity of OM arriving at the seafloor, as reflected in the smaller μ

380   values (Fig. 9A). In ocean areas characterized by pronounced OMZs, however, due to

381   strong coastal upwelling or a high export rate of plankton-derived OM, the inhibition of

382   OM degradation processes in the water colcunm results in the preservation of

20

383   heterogeneously mixed OM components (both active and refractory), as reflected in the

384   larger σ values (Fig. 9B), leading to higher than expected OM reactivity in specific regions

385   despite greater water depths (e.g., ARBS and EWTP ($<K_{region}> \approx 0.01$ yr^{-1}) (Fig. 9C). Thus,

386   the l-RCM provides a new framework not only for identifing the differences in OM

387   reactivity between regions, but also for assessing regional/global OM reactivity patterns

388   using easily obtainable information (e.g., sedimentation).

389   OM reactivity exerts an important control on the relative significance of OM degradation

390   pathways in marine sediments. In oxic environments, OM will be mainly respired

391   aerobically and through denitrification, whereas deeper within the sediment, it will mainly

392   be decomposed through anaerobic pathways such as sulfate reduction and methanogenesis

393   (Regnier et al., 2011). Therefore, further work should be conducted to simulate the

394   associated biogeochemical processes using the l-RCM to better quantify OM degradation

395   and burial in marine sediments on regional or global scales.

396
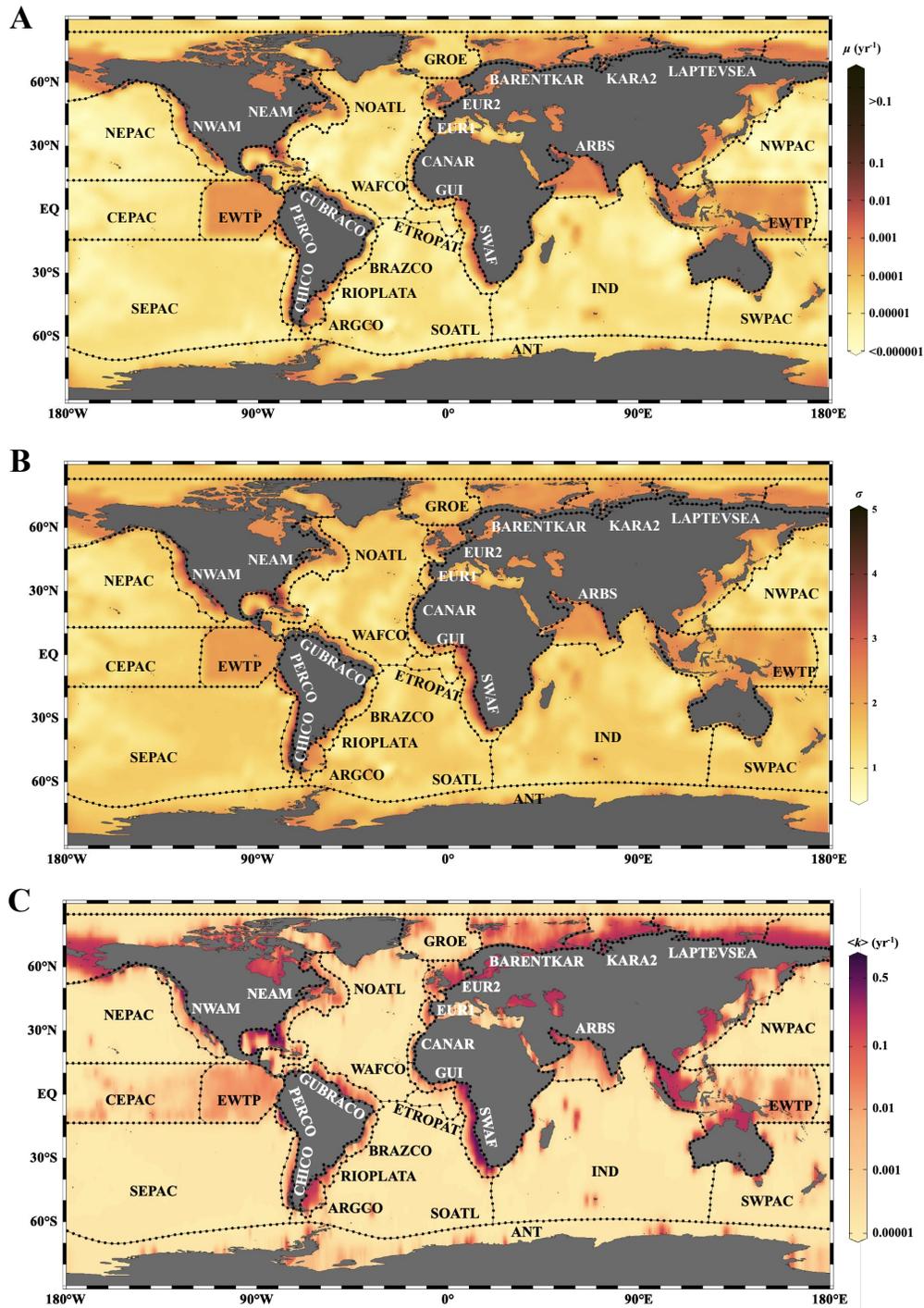
Figure 9. Distribution of μ (A), σ (B), and $<k>$ (C) in the global ocean with $1° \times 1°$ resolution.

401 **Table 2. Abbreviations of regions in this paper (Seiter et al., 2004), and their area,**
402 **mean water depth, mean OM content in surface sediment (<5 cm), and apparent OM**
403 **degradation rata (<K_{region}>).**

Abbreviation	Region	water depth[a] (m)	Mean OM (wt.%)	<K_{region}> (yr^{-1})
SWAF	SW-Africa continental margin	334	2.5	0.48542
NWAM	NW-America continental margin	731	1.7	0.12695
ARBS	Arabian Sea	1600	1.4	0.08182
EWTP	East-West Coastal Equatorial Pacific	3662	1.2	0.01587
ANT	South Polar Sea	1300	0.3	0.00029
ARGCO	Argentina continental margin	1859	0.3	0.00026
BARENTKAR	Barents Sea and Kara Sea	224	1.1	0.02081
BRAZCO	Brazil continental margin	1051	0.5	0.00034
CANAR	Canaries	1190	0.6	0.00031
CEPAC	Central Equatorial Pacific	5022	0.3	0.00002
CHICO	Chile continental margin	1444	1.5	0.00028
ETROPAT	Eastern tropical Atlantic	2253	0.7	0.00026
EUR1	N-European continental margin	1290	0.8	0.00029
EUR2	S-European continental margin	974	0.3	0.00037
GROE	Northern Nordic Sea	1563	0.7	0.00027
GUBRACO	SE-America continental margin	1844	0.4	0.00026
GUI	Gulf of Guinea	1586	1.1	0.00027
INA	Indian Ocean deep sea	4042	0.4	0.00021
KARA2	Kara Sea	281	1.2	0.01111
LAPTEVSEA	Laptev Sea	190	0.9	0.02964
NEAM	NE-America continental margin	1045	0.9	0.00034
NEPAC	NE-Pacific	4463	0.4	0.00012
NOATL	Northern Atlantic	2161	0.4	0.00026
NWPAC	NW-Pacific	4898	0.6	0.00004
PERCO	Peru continental margin	1020	4.8	0.00035
RIOPLATA	Rio de la Plata mouth	1784	0.8	0.00026
SEPAC	SE-Pacific	3952	0.5	0.00022
SOATL	Southern Atlantic	3592	0.4	0.00024
SWPAC	SW-Pacific	3153	0.8	0.00025
WAFCO	W-Africa continental margin	1982	0.6	0.00026

404 [a]water depth and mean OM content are based on the average depth and OM content of the
405 sites in each region of Fig.4.

406

407 **4 Conclusions**

408   Compared with previous OM degradation models, the *l*-RCM presented here not only

409   well fits OM depth-content profiles, but also better represents the distribution of OM

410   reactivity by the parameters μ and σ. We use the *l*-RCM to inversely determine μ and σ at

411   123 sites across the global ocean, including shelf, slope, and abyssal regions. Our results

412   show that the apparent OM reactivity ($<k>=\mu\cdot\exp(\sigma^2/2)$) decreases with decreasing

413   sedimentation rate (ω), and that OM reactivity is more than three orders of magnitude

414   higher in shelf than in abyssal regions. Due to the complex depositional environments (e.g.,

415   oxygen minimum zones), OM reactivity is higher than predicted in some specific regions

416   (e.g., the NWAM, SWAF, ARBS, and EWTP), which was also captured by the *l*-RCM in

417   these regions. Based on two empirical relationships between the OM reactivity ($<k>$) and

418   sedimentation rate (ω), we obtained the global OM reactivity distribution patterns and

419   finally mapped the global OM reactivity distribution. The reactivity of OM serving as fuel

420   for microbial activity in marine sediments firmly controls the degradation pathways and

421   metabolism rates. Thus, the *l*-RCM has direct implications on the constraints for OM

422   degradation and burial in marine sediments on regional or global scales.

423

424   **References**

425   Aller, R. C.: Bioturbation and remineralization of sedimentary organic matter: effects of
426   redox oscillation, Chem Geol, 114, 331-345, doi:10.1016/0009-2541(94)90062-0,
427   1994.
428   Aris, R.: Prolegomena to the rational analysis of systems of chemical reactions II. Some
429   addenda, Archive for Rational Mechanics and Analysis, 27, 356-364,
430   doi:10.1007/BF00282276, 1968.
431   Arndt, S., Jørgensen, B. B., LaRowe, D. E., Middelburg, J., Pancost, R., and Regnier, P.:
432   Quantifying the degradation of organic matter in marine sediments: a review and
433   synthesis, Earth-science reviews, 123, 53-86, doi:10.1016/j.earscirev.2013.02.008,
434   2013.

435 Berg, P., Rysgaard, S., Thamdrup, B.,: Dynamic modeling of early diagenesis and nutrient
436   cycling. A case study in an Arctic marine sediment, American Journal of Science 303,
437   905–955, doi: 10.2475/ajs.303.10.905, 2003.
438 Berner, R. A.: An idealized model of dissolved sulfate distribution in recent sediments,
439   Geochimica et Cosmochimica Acta, 28, 1497-1503, doi:10.1016/0016-7037(64)90164-
440   4, 1964.
441 Bogus, K. A., Zonneveld, K. A., Fischer, D., Kasten, S., Bohrmann, G., and Versteegh, G.
442   J.: The effect of meter-scale lateral oxygen gradients at the sediment-water interface on
443   selected organic matter based alteration, productivity and temperature proxies,
444   Biogeosciences, 9, 1553-1570, doi:10.5194/bg-9-1553-2012, 2012.
445 Boudreau, B. P.: A kinetic model for microbic organic-matter decomposition in marine
446   sediments, FEMS microbiology ecology, 11, 1-14, doi:10.1111/j.1574-
447   6968.1992.tb05789.x, 1992.
448 Boudreau, B. P.: A method-of-lines code for carbon and nutrient diagenesis in aquatic
449   sediments, Computers & Geosciences, 22, 479-496, doi:10.1016/0098-
450   3004(95)00115-8, 1996.
451 Boudreau, B. P., Arnosti, C., Jørgensen, B. B., and Canfield, D. E.: Comment on" Physical
452   model for the decay and preservation of marine organic carbon", Science, 319(5870),
453   1616-1616, doi:10.1126/science.1148589, 2008.
454 Boudreau, B. P. and Ruddick, B. R.: On a reactive continuum representation of organic
455   matter diagenesis, American Journal of Science, 291, 507-538,
456   doi:10.2475/ajs.291.5.507, 1991.
457 Bradley, J., Arndt, S., Amend, J., Burwicz, E., Dale, A. W., Egger, M., and LaRowe, D. E.:
458   Widespread energy limitation to life in global subseafloor sediments, Science advances,
459   6, doi:10.1126/sciadv.aba0697, 2020.
460 Burdige, D. J.: Preservation of organic matter in marine sediments: controls, mechanisms,
461   and an imbalance in sediment organic carbon budgets?, Chem Rev, 107, 467-485,
462   doi:10.1021/cr050347q, 2007.
463 Burwicz, E. B., Rüpke, L., and Wallmann, K.: Estimation of the global amount of
464   submarine gas hydrates formed via microbial methane formation based on numerical
465   reaction-transport modeling and a novel parameterization of Holocene sedimentation,
466   Geochimica et Cosmochimica Acta, 75, 4562-4576, doi:10.1016/j.gca.2011.05.029,
467   2011.
468 Cael, B., Bisson, K., and Follett, C. L.: Can rates of ocean primary production and
469   biological carbon export be related through their probability distributions?, Global
470   biogeochemical cycles, 32, 954-970, doi:10.1029/2017GB005797, 2018.
471 Dickens, A. F., Gelinas, Y., Masiello, C. A., Wakeham, S., and Hedges, J. I.: Reburial of
472   fossil organic carbon in marine sediments, Nature, 427, 336-339,
473   doi:10.1038/nature02299, 2004.
474 Dunne, J. P., Sarmiento, J. L., and Gnanadesikan, A.: A synthesis of global particle export
475   from the surface ocean and cycling through the ocean interior and on the seafloor, Global
476   Biogeochemical Cycles, 21, doi:10.1029/2006GB002907, 2007.
477 Egger, M., Riedinger, N., Mogollón, J. M., and Jørgensen, B. B.: Global diffusive fluxes
478   of methane in marine sediments, Nature Geoscience, 11, 421-425,
479   doi:10.1038/s41561-018-0122-8, 2018.

480 Forney, D. and Rothman, D.: Inverse method for estimating respiration rates from decay
481   time series, Biogeosciences, 9, 3601-3612, doi:10.5194/bg-9-3601-2012, 2012a.
482 Forney, D. C. and Rothman, D. H.: Common structure in the heterogeneity of plant-matter
483   decay, Journal of The Royal Society Interface, 9, 2255-2267,
484   doi:10.1098/rsif.2012.0122, 2012b.
485 Forney, D. C., and Rothman, D. H.: Carbon transit through degradation networks,
486   Ecological Monographs, 84(1), 109-129, doi: 10.1890/12-1846.1, 2014.
487 Freitas, F. S., Pika, P. A., Kasten, S., Jørgensen, B. B., Rassmann, J., Rabouille, C., Thomas,
488   S., Sass, H., Pancost, R. D., and Arndt, S.: Advancing on large-scale trends of apparent
489   organic matter reactivity in marine sediments and patterns of benthic carbon
490   transformation, Biogeosciences Discussions, 2021, 1-64, doi:10.5194/bg-18-4651-2021,
491   2021.
492 Garber, J. H.: Laboratory study of nitrogen and phosphorus remineralization during the
493   decomposition of coastal plankton and seston, Estuarine, Coastal and Shelf Science, 18,
494   685-702, doi:10.1016/0272-7714(84)90039-8, 1984.
495 Griffith, D. R., Martin, W. R., and Eglinton, T. I.: The radiocarbon age of organic carbon
496   in marine surface sediments. Geochimica et Cosmochimica Acta, 74(23), 6788-6800,
497   doi:10.1016/j.gca.2010.09.001, 2010.
498 Hammond, D., McManus, J., Berelson, W., Kilgore, T., and Pope, R.: Early diagenesis of
499   organic material in equatorial Pacific sediments: stpichiometry and kinetics, Deep Sea
500   Research Part II: Topical Studies in Oceanography, 43, 1365-1412, doi:10.1016/0967-
501   0645(96)00027-6, 1996.
502 Hartnett, H. E., Keil, R. G., Hedges, J. I., and Devol, A. H.: Influence of oxygen exposure
503   time on organic carbon preservation in continental margin sediments, Nature, 391(6667),
504   572-575, doi:10.1038/35351, 1998.
505 Hedges, J. I. and Keil, R. G.: Sedimentary organic matter preservation: an assessment and
506   speculative synthesis, Marine chemistry, 49, 81-115, doi:10.1016/0304-4203(95)00008-
507   F, 1995.
508 Hewson, I., Barbosa, J. G., Brown, J. M., Donelan, R. P., Eaglesham, J. B., Eggleston, E.
509   M., and LaBarre, B. A.: Temporal dynamics and decay of putatively allochthonous and
510   autochthonous viral genotypes in contrasting freshwater lakes, Applied and
511   environmental microbiology, 78, 6583-6591, doi:10.1128/AEM.01705-12, 2012.
512 Ho, T. and Aris, R.: On apparent second‐order kinetics, AIChE journal, 33, 1050-1051,
513   doi:10.1002/aic.690330621, 1987.
514 Ingole, B. S., Sautya, S., Sivadas, S., Singh, R., and Nanajkar, M.: Macrofaunal community
515   structure in the western Indian continental margin including the oxygen minimum zone,
516   Marine Ecology, 31, 148-166, doi:10.1111/j.1439-0485.2009.00356.x, 2010.
517 Jørgensen, B.: A comparison of methods for the quantification of bacterial sulfate reduction
518   in coastal marine sediments. II. Calculation from mathematical models, Geomicrobiol.
519   J, 1, 29-47, doi:10.1080/01490457809377721, 1978.
520 Jørgensen, B.: Processes at the sediment-water interface, The major biogeochemical cycles
521   and their interactions, 477-509, 1983.
522 Jørgensen, B. B., Wenzhöfer, F., Egger, M., and Glud, R. N.: Sediment oxygen
523   consumption: Role in the global marine carbon cycle, Earth-science reviews, 228,
524   103987. doi:10.1016/j.earscirev.2022.103987, 2022.

525 Kallmeyer, J., Pockalny, R., Adhikari, R. R., Smith, D. C., and D'Hondt, S.: Global
526   distribution of microbial abundance and biomass in subseafloor sediment,
527   Proceedings of the National Academy of Sciences, 109(40), 16213-16216, doi:
528   10.1073/pnas.1203849109, 2012.
529 Katsev, S. and Crowe, S. A.: Organic carbon burial efficiencies in sediments: The power
530   law of mineralization revisited, Geology, 43, 607-610, doi:10.1130/G36626.1, 2015.
531 Krumins, V., Gehlen, M., Arndt, S., Van Cappellen, P., and Regnier, P.: Dissolved
532   inorganic carbon and alkalinity fluxes from coastal marine sediments: model estimates
533   for different shelf environments and sensitivity to global change, Biogeosciences, 10,
534   371-398, doi:10.5194/bg-10-371-2013, 2013.
535 LaRowe, D., Arndt, S., Bradley, J., Estes, E., Hoarfrost, A., Lang, S., Lloyd, K., Mahmoudi,
536   N., Orsi, W., and Walter, S. S.: The fate of organic carbon in marine sediments-New
537   insights from recent data and analysis, Earth-Science Reviews, 204, 103146,
538   doi:10.1016/j.earscirev.2020.103146, 2020a.
539 LaRowe, D. E., Arndt, S., Bradley, J. A., Burwicz, E., Dale, A. W., and Amend, J. P.:
540   Organic carbon and microbial activity in marine sediments on a global scale throughout
541   the Quaternary, Geochimica et Cosmochimica Acta, 286, 227-247,
542   doi:10.1016/j.gca.2020.07.017, 2020b.
543 Limpert, E., Stahel, W. A., and Abbt, M.: Log-normal distributions across the sciences:
544   keys and clues: on the charms of statistics, and how mechanical models resembling
545   gambling machines offer a link to a handy way to characterize log-normal distributions,
546   which can provide deeper insight into variability and probability—normal or log-normal:
547   that is the question, BioScience, 51, 341-352, doi:10.1641/0006-
548   3568(2001)051[0341:LNDATS]2.0.CO;2, 2001.
549 Luff, R., Wallmann, K., and Aloisi, G.: Numerical modeling of carbonate crust formation
550   at cold vent sites: significance for fluid and methane budgets and chemosynthetic
551   biological communities. Earth and Planetary Science Letters, 221, 1-4, 337-353. doi:
552   10.1016/S0012-821X(04)00107-4, 2004.
553 Luff, R., Wallmann, K., Grandel, S., and Schlüter, M.: Numerical modeling of benthic
554   processes in the deep Arabian Sea, Deep Sea Research Part II: Topical Studies in
555   Oceanography, 47, 3039-3072, doi:10.1016/S0967-0645(00)00058-8, 2000.
556 Meister, P., Herda, G., Petrishcheva, E., Gier, S., Dickens, G. R., Bauer, C., and Liu, B.:
557   Microbial alkalinity production and silicate alteration in methane charged marine
558   sediments: Implications for porewater chemistry and diagenetic carbonate formation,
559   Frontiers in Earth Science, 9: 756591, doi:10.3389/feart.2021.756591, 2022.
560 Meysman, F. J., Middelburg, J. J., Herman, P. M., and Heip, C. H.: Reactive transport in
561   surface sediments. II. Media: an object-oriented problem-solving environment for early
562   diagenesis, Computers & geosciences, 29, 301-318, doi:10.1016/S0098-
563   3004(03)00007-4, 2003.
564 Middelburg, J. J.: A simple rate model for organic matter decomposition in marine
565   sediments, Geochimica et Cosmochimica acta, 53, 1577-1581, 10.1016/0016-
566   7037(89)90239-1, doi:10.1016/0016-7037(89)90239-1, 1989.
567 Middelburg, J. J., Soetaert, K., and Herman, P. M.: Empirical relationships for use in global
568   diagenetic models, Deep Sea Research Part I: Oceanographic Research Papers, 44, 327-
569   344, doi:10.1016/S0967-0637(96)00101-X, 1997.

570 Mollenhauer, G., Eglinton, T. I., Ohkouchi, N., Schneider, R. R., Müller, P. J., Grootes, P.
571   M., and Rullkötter, J.: Asynchronous alkenone and foraminifera records from the
572   Benguela Upwelling System, Geochimica et cosmochimica acta, 67, 2157-2171,
573   doi:10.1016/S0016-7037(03)00168-6, 2003.

574 Müller, P. J. and Suess, E.: Productivity, sedimentation rate, and sedimentary organic
575   matter in the oceans—I. Organic carbon preservation, Deep Sea Research Part A.
576   Oceanographic Research Papers, 26, 1347-1362, doi:10.1016/0198-0149(79)90003-7,
577   1979.

578 Munhoven, G.: Glacial–interglacial rain ratio changes: Implications for atmospheric CO2
579   and ocean–sediment interaction, Deep Sea Research Part II: Topical Studies in
580   Oceanography, 54, 722-746, doi:10.1016/j.dsr2.2007.01.008, 2007.

581 Nöthen, K., Kasten, S.,: Reconstructing changes in seep activity by means of pore water
582   and solid phase Sr/Ca and Mg/Ca ratios in pockmark sediments of the Northern Congo
583   Fan, Marine Geology, 287(1-4): 1-13, doi:10.1016/j.margeo.2011.06.008, 2011.

584 Pika, P., Hülse, D., and Arndt, S.: OMEN-SED (-RCM)(v1. 1): a pseudo-reactive
585   continuum representation of organic matter degradation dynamics for OMEN-SED,
586   Geoscientific Model Development, 14, 7155-7174, doi:10.5194/gmd-14-7155-2021,
587   2021.

588 Regnier, P., Dale, A. W., Arndt, S., LaRowe, D. E., Mogollón, J., and Van Cappellen, P.:
589   Quantitative analysis of anaerobic oxidation of methane (AOM) in marine sediments: A
590   modeling perspective, Earth-Science Reviews, 106(1-2), 105-130,
591   doi:10.1016/j.earscirev.2011.01.002, 2011.

592 Rowe, G. T. and Staresinic, N.: Sources of organic matter to the deep-sea benthos, Ambio
593   Special Report, 19-23, doi:10.2307/25099603, 1979.

594 Seiter, K., Hensen, C., Schröter, J., and Zabel, M.: Organic carbon content in surface
595   sediments—defining regional provinces, Deep Sea Research Part I: Oceanographic
596   Research Papers, 51, 2001-2026, doi:10.1016/j.dsr.2004.06.014, 2004.

597 Smith, S. and Hollibaugh, J.: Coastal metabolism and the oceanic organic carbon balance,
598   Reviews of Geophysics, 31, 75-89, doi:10.1029/92RG02584, 1993.

599 Volz, J. B., Mogollón, J. M., Geibert, W., Arbizu, P. M., Koschinsky, A., and Kasten, S.:
600   Natural spatial variability of depositional conditions, biogeochemical processes and
601   element fluxes in sediments of the eastern Clarion-Clipperton Zone, Pacific Ocean, Deep
602   Sea Research Part I: Oceanographic Research Papers, 140, 159-172,
603   doi:10.1016/j.dsr.2018.08.006, 2018.

604 Westrich, J. T. and Berner, R. A.: The role of sedimentary organic matter in bacterial
605   sulfate reduction: The G model tested 1, Limnology and oceanography, 29, 236-249,
606   doi:10.4319/lo.1984.29.2.0236, 1984.

607 Whiticar, M. J.: Carbon and hydrogen isotope systematics of bacterial formation and
608   oxidation of methane. Chemical geology, 161, 291–314. doi: 10.1016/S0009-
609   2541(99)00092-3, 1999.

610 Zonneveld, K. A., Versteegh, G. J., Kasten, S., Eglinton, T. I., Emeis, K.-C., Huguet, C.,
611   Koch, B. P., de Lange, G. J., de Leeuw, J. W., and Middelburg, J. J.: Selective
612   preservation of organic matter in marine environments; processes and impact on the
613   sedimentary record, Biogeosciences, 7, 483-511, doi:10.5194/bg-7-483-2010, 2010.

614

Author contributions

S.X. and B.L. designed the study and performed the research with S.A., S.K., and Z.W.; All authors discussed the results and commented on the manuscript.

Competing interests

The authors declare that they have no competing interests.